The Astrophysical Journal, 192: 351–368, 1974 September 1

COMPACT INFRARED SOURCES ASSOCIATED WITH SOUTHERN H II REGIONS

Jay A. Frogel* and S. Eric Persson*
Center for Astrophysics, Harvard College Observatory and Smithsonian Astrophysical Observatory
Received 1974 January 22

ABSTRACT

We have found bright, compact, infrared (1–25 μ) sources associated with 11 galactic H II regions. We present maps showing complex structure at 10 μ in five of these sources. The remaining ones are characterized by a small ($< 20''$) core of high surface brightness, with an extended ($\sim 1'$) halo.

RCW 57/IRS 1, an unresolved source exceptionally bright at 4.8 μ, may be a protostar; a similar object may be embedded in RCW 38/IRS 1. The 1–25 μ luminosity of the single-component source G298.2−0.3 is $2 \times 10^6 L_\odot$, the highest of any known H II region. In one source we have been able to detect the exciting star (RCW 38/IRS 2).

As is typical for H II regions with infrared counterparts, the energy spectra from 1.2 to 20 μ are at least as steep as $F_\nu \propto \nu^{-3}$, and the observed flux longward of 3.5 μ is in excess, while that shortward of 2.2 μ is deficient when compared with an extrapolation of the radio fluxes. The short-wavelength data show that most of the sources are more heavily reddened than would be expected from interstellar dust alone. For any given source the colors at all wavelengths do not vary significantly with position, implying that the dust which radiates in the 10–20 μ region is well mixed with the ionized gas. Also, we find for this dust a lower limit to the ratio M(H II)/M(dust), which, for a reasonable choice of physical parameters, is higher than the interstellar value.

The optical depth of a 10-μ absorption feature usually associated with silicates correlates with $\tau(H_2CO)$ as determined from radio measurements but not with the visual extinction. We attribute the radio and 10-μ absorption features to cool dust and molecules in circumnebular neutral clouds. The dust in these clouds is probably responsible for the far-infrared radiation, as has been discussed by several authors.

For most and possibly for all the H II regions, the 1–25 μ flux can be accounted for by the absorption on dust grains of resonantly trapped Lα photons. We find no evidence that any of this dust markedly affects the ionization structure of the H II regions.

Subject headings: infrared sources — interstellar matter — nebulae

I. INTRODUCTION

We have detected strong emission in the 1–20 μ region from 11 southern galactic radio sources which have been identified as H II regions by Goss and Shaver (1970) and Caswell (1972). The sources were selected for observation in the infrared on the basis of their high emission measure ($> 5 \times 10^5$ cm^{-6} pc) and small angular size ($<$ a few arc minutes). We discussed two additional ones in detail (Becklin *et al.* 1973*a*, 1974) and all 13 briefly (Persson and Frogel 1973; Frogel and Persson 1973). In this paper we present high spatial-resolution data and spectral-energy distributions in the range 1.25–20 μ for the 11 new sources and point out the nondetection of one other radio source. We also present preliminary observations of the 10-μ absorption feature which has been observed in other H II regions (Gillett and Forrest 1973).

Only a limited amount of radio interferometric observations are available for the sources discussed in this paper (Balick 1972; Brown and Broderick 1974). Thus, it has been impossible to make a detailed comparison between radio and infrared observations such as has been done by Kleinmann (1973) and Wynn-Williams, Becklin, and Neugebauer (1972, 1974*a*). However, for the purposes of interpretation we shall assume, as we did for G333.6−0.2 and H2-3 (Becklin *et al.* 1973*a*, 1974), that all of the compact infrared sources, with the exceptions of RCW 57/IRS 1 and RCW 38/IRS 2, have compact radio-continuum counterparts. Justification for this assumption will become apparent in the following sections.

We have addressed ourselves to the following questions: What are the relative and absolute distributions and masses of the gas and dust? Are there any correlations between absorption features seen in the infrared and radio and the visual extinction? What are the energetics of the interactions between gas, dust, and starlight? The observational procedure is described in § II, and the observed properties of each source are presented in § III. A source which we identify as an early-type star in RCW 38 is discussed in § IV. A possible protostar in RCW 57 is discussed in § V. In §§ VI and VII we consider the reddening and extinction of the sources, and discuss the properties of the infrared emission as they relate to the questions posed above. A summary of the observations and results is given in § VIII.

II. OBSERVATIONS AND DATA REDUCTION

All of the observations were obtained with the 1-m telescope of the Carnegie Institution of Washington at Las Campanas, Chile, in 1972 April and 1973 March. Some of the 10- and 20-μ photometric observations of RCW 38, RCW 57, and RCW 97 were made by Becklin

* Guest Investigator, Las Campanas Observatory, Carnegie Institution of Washington.

TABLE 1

Observed Properties of H II Regions

No.	Galactic Source	Other* Names	Radio Position (1950.0)	10-μ† Position (1950.0)	Size (arc min) Radio FWHP	Size (arc min) IR‡	Dist. (kpc)	Log F_ν (W m^{-2} Hz^{-1}) 5 GHz	Log F_ν (W m^{-2} Hz^{-1}) 10 μ‡	Log $\left(\frac{L_\alpha}{L_\odot}\right)$	Log $\left[\frac{L(1\text{–}25\,\mu)}{L_\odot}\right]$	A_V $\left(\frac{2.2\,\mu}{\text{radio}}\right)$	A_V $\left(\frac{1.65\,\mu}{2.2\,\mu}\right)$	Notes
1....	G268.0−1.1	RCW 38, CTB 31	08ʰ57ᵐ23ˢ −47°19′.4	08ʰ57ᵐ24ˢ.2 −47°18′50″	1.7	1.8	1.5	−23.76	−22.88	5.15	4.98	+19.8	10.7	1, 3, 10, 15
2....	G284.3−0.3	RCW 49, NGC 3247	10 22 20 −57 32.0	10 22 10 −57 30 30	5.5	1.7 × 4	6	−23.75	−23.11	6.40	5.85	>46	...	1, 3, 4, 10, 16
3....	G285.3−0.0		10 29 37 −57 46.7	10 29 35.7 −57 46 37	1.9	(1.0)	5	−24.78	(−24.24)	5.32	4.57	+22.6	5.0	1, 3, 11, 15, 17
4....	G291.3−0.7	RCW 57, NGC 3576	11 09 46 −61 02.6	11 09 46.3 −61 02 09	1.1	1.5	3.6	−24.01	−23.10	5.68	5.53	+13.6	14.9	1, 3, 10, 16
5....	G298.2−0.3		12 07 24 −62 33.3	12 07 22.5 −62 33 20	2.0	1.1	12	−24.51	−23.34	6.20	6.25	+21.2	14.0	1, 3, 10, 14, 18
6....	G327.3−0.6	RCW 97	15 49 12 −54 26.5	15 49 12.9 −54 26 27	1.0	2	3.4	−24.35	−23.50	5.51	4.99	+20.6	20.0	1, 3, 10, 15, 17
7....	G333.3−0.4		16 17 45 −50 19.3	16 17 44.1 −50 18 02	1.8	(1.0)	3.8	−24.47	(−23.91)	5.34	4.77	+31.6	...	1, 5, 11
8....	G333.6−0.2		16 18 26 −49 58.9	16 18 27.1 −49 58 54	1.1	1.0	4.5	−24.07	−22.81	5.81	5.86	+17.2	17.7	1, 3, 13, 17
9....	G336.5−1.5	RCW 108, NGC 6193	16 36 22 −48 46.3	16 36 14.6 −48 45 53	0.7	1.0	2.1	−25.07	−23.75	4.10	4.62	− 0.6	10.9	1, 6, 10, 14
10....	G345.4−0.9	RCW 117, H2-3	17 06 08 −41 31.9	17 06 01.5 −41 32 20	1.7	2.0	5	−24.47	−23.30	5.48	5.45	+ 6.2	9.0	2, 3, 13
11....	G351.6−1.3		17 25 56 −36 37.5	17 25 53.0 −36 37 49	2.4 (<1)	(1.0)	5	−24.54 (−25.24)	(−24.12)	5.58 4.88)	4.68	+32.8 (15.3)	...	2, 3, 7, 11, 15
12....	G353.2+0.9	W22, NGC 6357	17 21 30 −34 08.3	17 21 24.1 −34 08 24	3 (2.5)	1.5 × 4	1.0	−24.06 (24.47)	−22.77	4.53 (4.12)	4.58	+32.5 (21.1)	...	1, 6, 8, 10
13....	G12.8−0.2	W33	18 11 17 −17 56.9	18 11 18.3 −17 57 30	0.8 (0.2)	1.0	4.6	−24.57 (−25.30)	−24.59	5.35 (4.62)	4.24	+50.4 (29.1)	...	1, 3, 9, 12, 17, 19

* RCW indicates an optical identification from the catalog of Rodgers, Campbell, and Whiteoak (1960).

† The errors in the 10-μ positions are typically ±4″. For multiple-component sources, the position refers to the component of highest surface brightness.

‡ Infrared size refers to area mapped. Values of infrared size or log F_2 (10μ) in parentheses refer to largest aperture used at 2.2 μ. See also note 11.

NOTES TO TABLE 1

1. Radio position from 5-GHz measurements by Goss and Shaver (1970); radio size and flux from Shaver and Goss (1970). Uncertainties in the position are typically ±1′.
2. Radio position, 5-GHz flux density, and size from Caswell (1972).
3. Distance from 21-cm observations of Radhakrishnan *et al.* (1972) or Goss *et al.* (1972).
4. Optical distance from Westerlund (1960) agrees with 21-cm distance.
5. Distance from Shaver and Goss (1970).
6. Distance is optically determined and quoted by Shaver and Goss (1970).
7. Numbers in parentheses refer to 85-GHz measurements of Brown and Broderick (1973). The (1950.0) 3.7-cm interferometric position (Brown and Broderick 1974) is $\alpha = 17^h25^m52^s.9$ ($\pm 0^s.4$), $\delta = -36°37'44''$ ($\pm 6''$).
8. Numbers in parentheses refer to 15-GHz measurements of Schraml and Mezger (1969) for a compact component which they have separated out from background.
9. Numbers in parentheses refer to 8-GHz measurements by Balick (1972) of compact component found with interferometer.
10. $F_\nu(10\,\mu)$ computed by integrating the map presented in text. $L(1\text{–}25\,\mu)$ computed from $F_\nu(10\,\mu)$ and spectrum as discussed in text.
11. The difference between measurements made with apertures 23″ and 59″ in diameter at 2.2 and/or 3.5 μ was used to scale up a 22″ aperture measurement made at 10μ to get $F_\nu(10\,\mu)$. These values are given in parentheses. $L(1\text{–}25\,\mu)$ computed as in note 10. Both of these quantities are probably underestimated.
12. Same as note 11, but probably no underestimate.
13. $F_\nu(10\,\mu)$ from Becklin *et al.* (1973*a* or 1974); $L(1\text{–}25\,\mu)$ computed as in note 10; no underestimate of values.
14. $F_\nu(10\,\mu)$ computed as in notes 10 and 11; the two agree to within 20 percent.
15. OH in emission at the radio position (Manchester, Robinson, and Goss 1970; or Robinson *et al.* 1971).
16. OH in absorption only at the radio position (Manchester *et al.* 1970).
17. H_2O in emission at or near the radio position (Johnston *et al.* 1972, or 1973).
18. Neither emission nor absorption from OH at the radio position (Manchester *et al.* 1970).
19. OH in emission 5′ away from radio positions (Robinson, Goss, and Manchester 1970; Wynn-Williams, Werner, and Wilson 1974*b*).

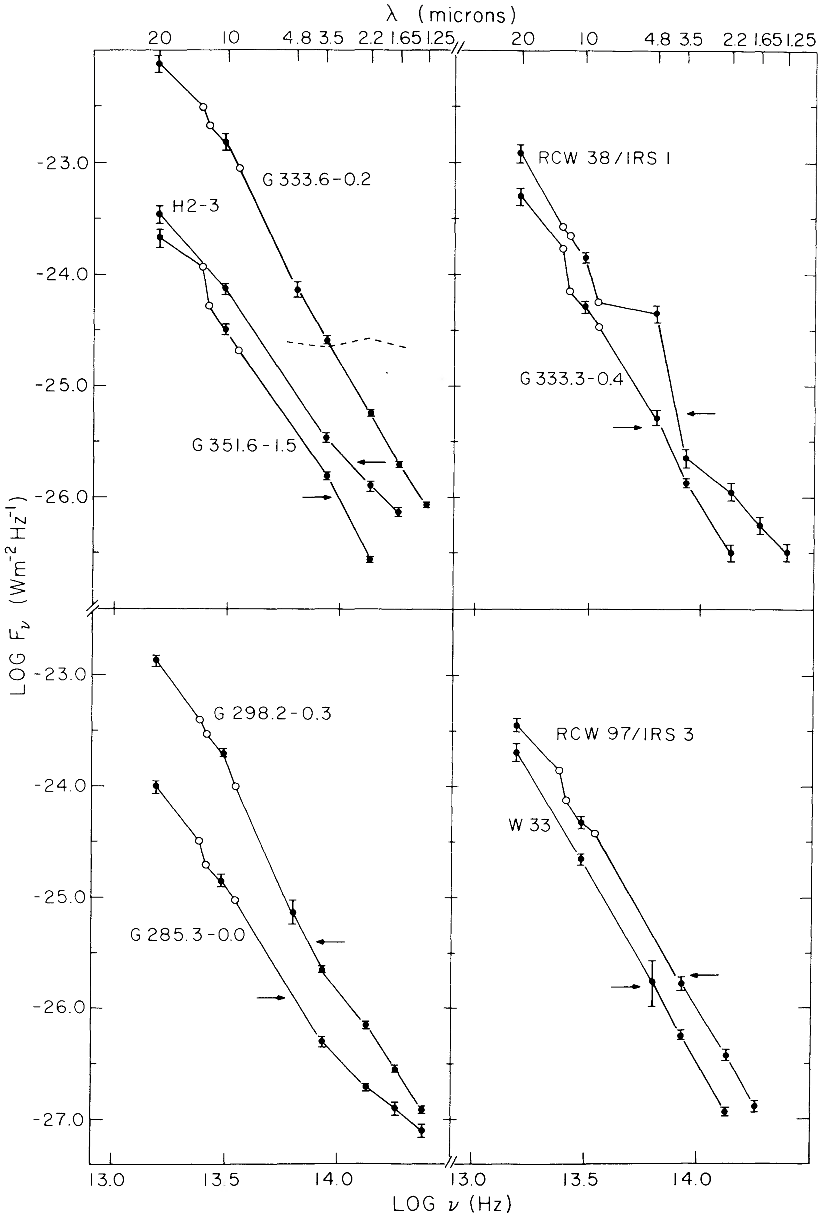

FIG. 1*a*

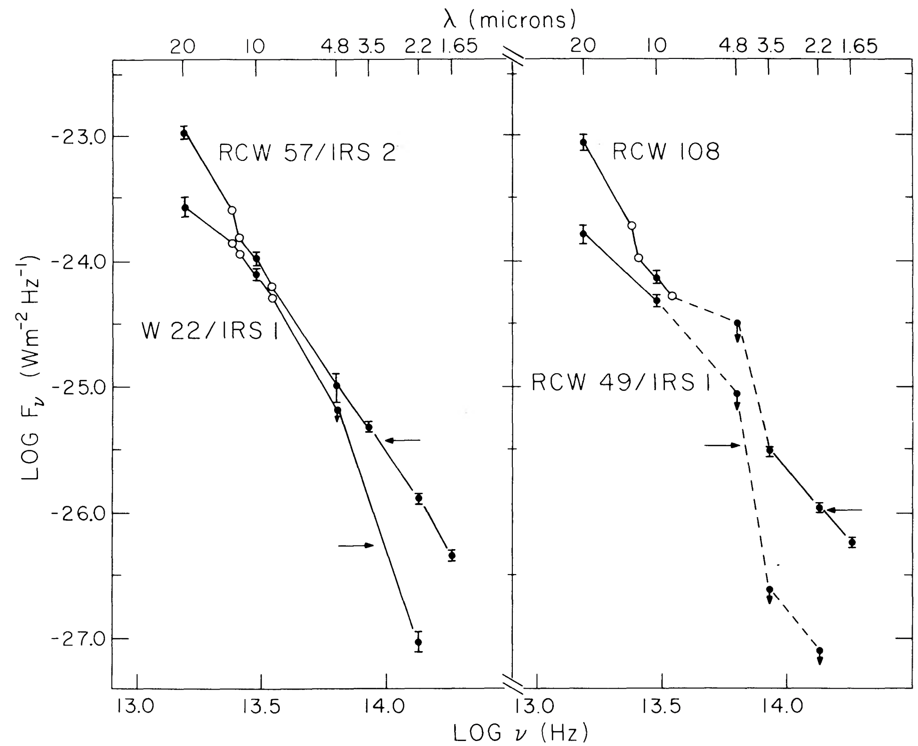

FIG. 1*b*

FIG. 1.—Spectral energy distributions for 13 H II regions. The measurements have been corrected for beam-size effects and for the extended nature of the sources. The error bars are 1 σ_m and include both statistical errors of the measurements and all other major sources of uncertainty. The measurements were made with an aperture diameter of 23″ with the following exceptions: a 14″.5 aperture, for W22 and RCW 38; 29″, for H2-3; 45″, for G333.6−0.2; the measurements for RCW 38/IRS 1 and RCW 57/IRS 2 exclude contributions from RCW 38/IRS 2 and RCW 57/IRS 1, respectively. Vertical arrows are 1 σ upper limits. Horizontal arrows are the predicted 2.2-μ emission levels for each source found from the radio data and the formulae of Willner *et al.* (1972). These predicted values have been scaled down to correspond to the aperture size used.

and Neugebauer in 1972 September with large-diameter apertures. The observations from 1.25 to 3.5 μ were made with a PbS photoconductor, and those from 4.8 to 20 μ with a Ge:Ga bolometer; both systems utilized cooled focal-plane apertures and filters. The central wavelengths and half-power bandwidths of the filters are: 1.25 μ, 0.28 μ; 1.65 μ, 0.30 μ; 2.2 μ, 0.41 μ; 3.5 μ, 0.57 μ; 4.8 μ, 0.52 μ; 8.7 μ, 0.95 μ; 10 μ, 5 μ; 11.7 μ, 2.56 μ; 12.6 μ, 1.23 μ; 20 μ, 10 μ. The calibration of the photometry is that given by Wilson *et al.* (1972).

The beam switching was accomplished by use of a sector-wheel chopper, for the 1.25–3.5 μ observations, and by wobbling the secondary mirror of the telescope, for those at the longer wavelengths. Beam separations were typically 73″ (or 116″) and 44″ for the short and long wavelengths, respectively. The smaller separations reduce the sensitivity to emission components that have relatively low surface-brightness gradients.

The observing procedure consisted, first, of scanning at 2.2 and/or 10 μ a region typically 5′ on a side centered on the 5-GHz radio continuum position. Those radio sources that exhibited complex infrared structure and were of relatively high surface brightness were then fully mapped at 10 μ with apertures of 14″.5 or 22″ diameter; some were partially mapped at 20 μ. The separation between adjacent scans was in all cases 14″.5. For the sources that showed little or no structure or were of low surface brightness, scans at 10 and 20 μ were made only through the position of maximum signal; it was necessary to co-add as many as eight scans to achieve an adequate signal-to-noise ratio. The scans were made in the same direction as the beam separation, viz., right ascension. Since the recorded signal is the difference in signal between the two beams, it was necessary to deconvolve the data in order to produce true intensity scans; the beam profile itself, however, was not deconvolved. Also, multiaperture photometry of all objects at all wavelengths was attempted on at least those areas that represented distinct peaks of infrared emission. Most of these peaks were also measured with three intermediate-bandwidth filters to determine the strength of an absorption feature at 10 μ which has been seen in other H II regions (Gillett and Forrest 1973).

The sources we have observed are listed in table 1. Positions were measured for all sources by offsetting from nearby field stars and subsequently determining the absolute positions of the field stars from plates either in the Harvard plate collection or various photographic atlases and the *Smithsonian Astrophysical Observatory Star Catalogue*.

The 10-μ flux densities (table 1) were found either by integrating the contour maps presented in § III, or by measuring the 2.2-μ flux with apertures of various sizes to predict the 10-μ flux which would be measured through a 59″ diameter aperture. This procedure is valid if the [2.2 μ] − [10 μ] color is independent of aperture size. This is true for the objects for which there are sufficient data. An alternative method for the sources for which only central scans at 10 μ were obtained is to assume circular symmetry and integrate under the central scans. The integrated 10-μ fluxes obtained by these latter two methods agree to within 20 percent. Two single-component sources were mapped at 10 μ and were measured with multiaperture photometry. Again, the different methods for obtaining the integrated 10-μ fluxes agreed to within 20 percent.

Both the full width at half-power (FWHP) radio size and the size of the region in which we have measured infrared emission are listed in table 1. The other entries in table 1 are discussed later.

III. DESCRIPTION OF INDIVIDUAL SOURCES

In this section we describe the infrared observations of each source and summarize the relevant radio continuum data. Molecular-line observations of OH and H_2O are noted in table 1. RCW 38, RCW 49, RCW 57, RCW 97, and W22 were found to have complex spatial structure and are discussed first. Six other sources, G285.3−0.0, G298.2−0.3, G333.3−0.4, RCW 108, G351.6−1.3, and W33 are discussed next. This group is characterized by a compact infrared source embedded in an extended envelope of considerably lower surface brightness. The sources discussed by Becklin *et al.* (1973*b*; 1974), G333.6−0.2 and H2-3, are of this type and we present new intermediate-band 10-μ data for G333.6−0.2. Finally, we discuss W31, a radio source not detected at 10 μ. Figure 1 displays the energy distributions of the sources.

a) RCW 38 (G268.0−1.1), RCW 57 (G291.3−0.7), and RCW 97 (G327.3−0.6)

RCW 38 and RCW 57 (NGC 3576) each consist of several optical components lying in obscured regions. They are both very bright 5-GHz sources (table 1), their peaks of radio emission lying in the obscured regions. RCW 97 (G327.3−0.6) is similar but its optical emission is considerably weaker.

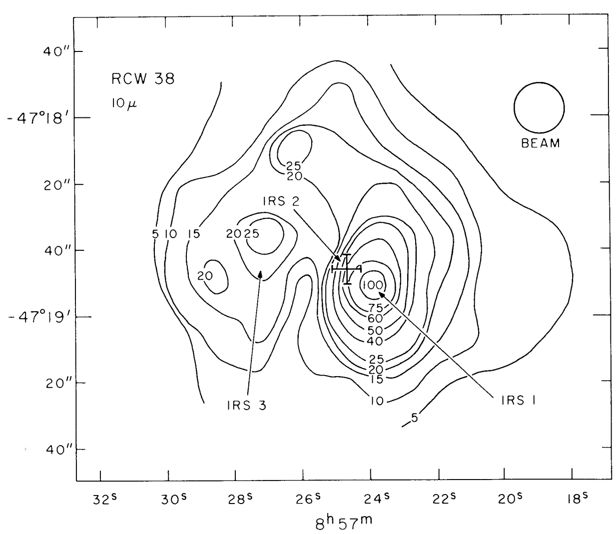

FIG. 2.—A 10-μ map of RCW 38. In this and all other maps, the FWHP beam size is shown by a circle and the coordinates are for epoch 1950.0. IRS 1 is the 10-μ and 5-GHz peak position and IRS 2 is the 2.2-μ peak. The flux density contours are in units of 100 = 1.5 × 10^{-24} W m^{-2} Hz^{-1} as measured with a 14″.5 diameter aperture. The central flux measured for IRS 1 is 108 in these units.

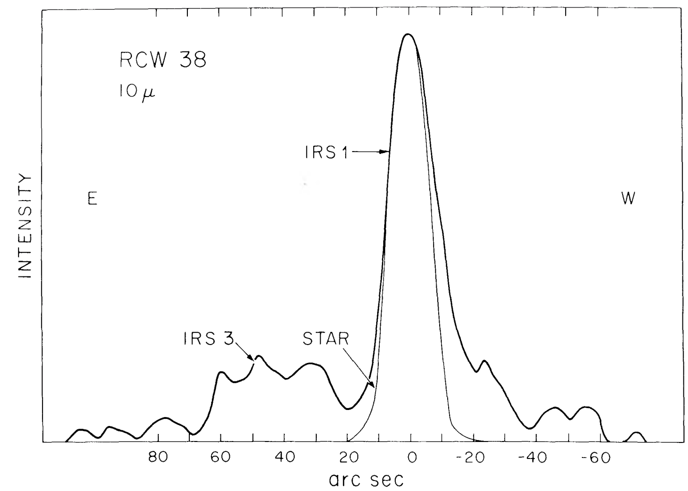

FIG. 3.—A representative deconcolved scan through RCW 38 at 10 μ. It passes through IRS 1 and to the south of IRS 3 at a declination of $\delta = -47°18'50''$. A 10-μ scan through a star is shown for comparison. The scan of the star in this plot and all other plots of this type in this paper are normalized to the peak intensity of the source. These scans were made with the same beam size used for the map.

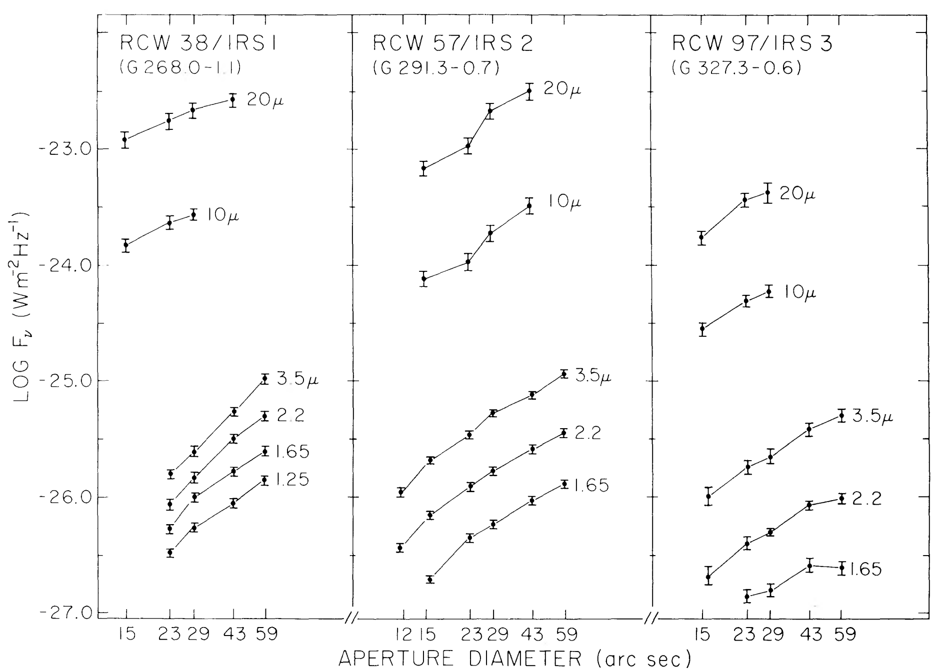

FIG. 4.—Relations between flux density and aperture diameter (plotted logarithmically) for three components of H II regions. A source of constant surface brightness would appear similar to RCW 38/IRS 1 at 3.5 μ. Note that for this source the short- and long-wavelength data cannot be compared directly, because, for $\lambda \leq 3.5$, multiaperture data were obtained with the apertures centered on IRS 2 and those at 10 and 20 μ were centered on IRS 1. For RCW 57/IRS 2 the flux from IRS 1 was subtracted from all measurements in order to display the color of the extended emission.

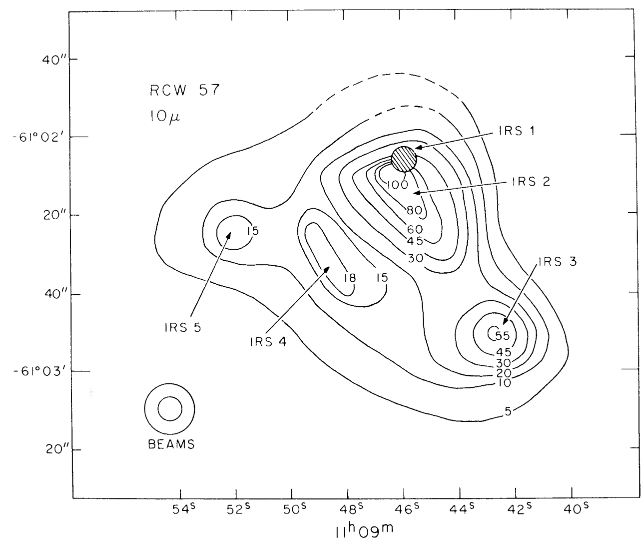

FIG. 5.—A 10-μ map of RCW 57 (component NGC 3576 only). IRS 1 is the source that is bright at 4.8 μ. Its position and flux were found by using the smaller beam size indicated. The flux density contours are in units of $100 = 1.1 \times 10^{-24}$ W m^{-2} Hz^{-1} as measured with a 14″.5 diameter aperture. The 5-GHz position is close to IRS 2. The position of the peak of RCW 57/IRS 2 relative to IRS 1 may be in error because the sources are close together and bright.

i) *RCW 38*

A map of the 10-μ emission associated with RCW 38 is shown in figure 2. A right ascension scan at 10 μ which passes through the peak of IRS 1 and south of IRS 3 is displayed in figure 3. Declination scans at 2.2 and 3.5 μ with a 23″ diameter aperture indicated a moderately bright source north of IRS 3, just outside the region mapped at 10 μ. Except near IRS 2, the 2.2- and 3.5-μ scans were similar to one another. Also, the distribution of emission at these wavelengths is similar to the distribution at 10 μ. In particular, the unmarked 10-μ local maximum north of IRS 3 (fig. 2) is also present at the shorter wavelengths.

The [10 μ] − [20 μ] color of RCW 38 does not change by more than 0.3 mag over the face of the object, as shown by photometry of IRS 1, IRS 3, a point NW of IRS 1, and multiaperture photometry of IRS 1 (fig. 4). Multiaperture photometry at 1.25, 1.65, 2.2, and 3.5 μ was done with apertures centered on RCW 38/IRS 2, a source which was not detected at wavelengths longer than 3.5 μ. This source dominates the fluxes measured through the smaller apertures. The colors that result when the fluxes measured through the smallest aperture (16″) are subtracted from those measured with each of the larger apertures are also independent of aperture size (fig. 4). The resulting fluxes cannot easily be compared with the 10- and 20-μ fluxes, however, because of the difference in centering and the steep gradient in 10-μ flux going from IRS 1 to IRS 2.

A grid of 12 points mostly S and W of IRS 2 was measured at 1.65, 2.2, and 3.5 μ. The [2.2 μ] − [3.5 μ] colors at these positions change by as much as 0.5 mag but not in a systematic manner. The multiaperture observations smooth out these small-scale color variations, and give an average color for the source.

In order to produce the spectral-energy distribution of RCW 38/IRS 1 shown in figure 1, we interpolated between the measured grid points. The multiaperture colors were used to derive the 1.25-μ flux of RCW 38/IRS 1.

Figure 3 shows that IRS 1 is a compact source with a FWHP of 9″ at 10 μ. The [4.8 μ] − [10 μ] color is considerably bluer than that of any source discussed in this paper except for the unresolved source RCW 57/IRS 1 (discussed in § V). Further observations are required to establish the similarity between the two sources.

RCW 38/IRS 2 is less than 10″ in diameter at 2.2 μ and, when measured with a 16″ diameter aperture, is by far the brightest 2.2-μ source in RCW 38. Its properties are discussed in § IV.

ii) *RCW 57*

A 10-μ map of RCW 57 is presented in figure 5. In addition to the scans made with a 14″.5 aperture, scans with a 7″ aperture were made in the area around IRS 1,

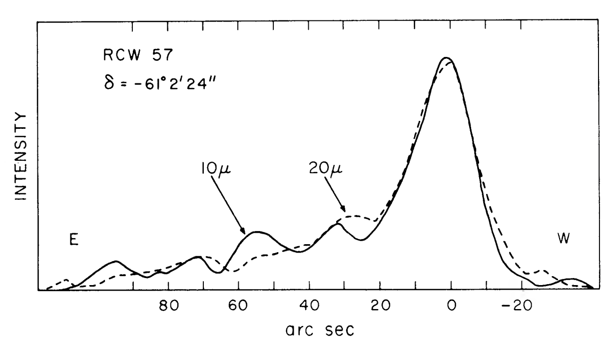

FIG. 6.—Representative 10- and 20-μ deconvolved scans through RCW 57. The similarity of the intensity distributions at these wavelengths is typical for this source.

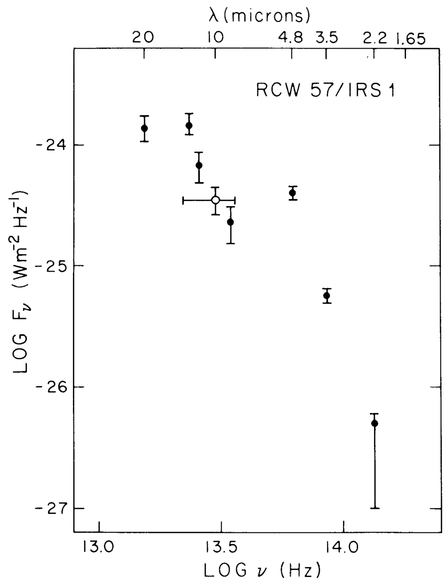

FIG. 7.—Spectral energy distribution of the unresolved 4.8-μ source in RCW 57/IRS 1. The open circle is the broad-band 10-μ measurement; the bandwidth of the filter is indicated by a horizontal bar. The data refer only to the point source itself and include no background emission. The weakness of IRS 1 relative to the 2.2-μ background results in a large uncertainty in the 2.2-μ flux density. These data can be fitted by a 390° K blackbody with large absorption in the 10-μ region.

IRS 2, and IRS 3. These scans confirmed the structure near the discrete sources, and did not resolve IRS 1 (< 3″). Scans of most of the region in figure 5 were made at 20 μ, and were not significantly different from those at 10 μ; figure 6 gives a typical comparison. Scans were also made through IRS 1 and IRS 2 at 2.2 and 3.5 μ with a 23″ aperture. At 3.5 and 4.8 μ an unresolved source corresponding in position (± 1″.5) with IRS 1 dominates the emission. Although considerably fainter at 2.2 μ, it is still clearly unresolved at this wavelength also. The spectral energy distribution of IRS 1 is shown in figure 7. The source is discussed in § V.

Multiaperture photometry at 1.65, 2.2, 3.5, 10, and 20 μ was carried out with apertures centered on IRS 2 and the results are plotted in figure 4. *It is clear that the dependence on flux on aperture is similar at all wavelengths*. This is shown to be true for other sources as well, and is an important observational result. Additional 10- and 20-μ measurements at selected points yielded the same color to within 0.1 mag as that indicated in figure 4. Finally, measurements of a grid of six points around RCW 57/IRS 1 showed that the [2.2 μ] − [3.5 μ] color varies by less than 0.3 mag.

iii) *RCW 97* (*G327.3−0.6*)

The 10-μ map of RCW 97 is shown in figure 8, and the spectrum of IRS 3 in figure 1; it is similar to those of RCW 38 and RCW 57. Multiaperture photometry of RCW 97 from 1.65 to 20 μ was done with apertures centered on IRS 3. These data are presented in figure 4. As in RCW 57, the dependence of flux on aperture is similar at all wavelengths. Photometry of RCW 97/IRS 1 at 10 and 20 μ yielded the same color as IRS 3, within the errors. One 20-μ scan, of considerably lower quality than the 10-μ scans, suggests that IRS 1 may be slightly more extended at the longer wavelength.

b) *RCW 49* (*G284.3−0.3*)

The infrared emission associated with this source lies to the south of the optical nebula RCW 49, and is considerably extended east-west (fig. 9). Additional right ascension scans through RCW 49/IRS 1 were made at 20 μ, and although of lower quality, they agreed with the 10-μ scans as to sizes and positions of features.

Because the source is very extended in a direction parallel to the scans, 10-μ declination scans were also made. These confirmed the long, continuous ridge of emission and showed that RCW 49/IRS 1 is unresolved (< 4″) in the declination direction. Although RCW 49 is the bluest source measured at 10 and 20 μ, only an upper limit to the 2.2-μ flux of RCW 49/IRS 1 of

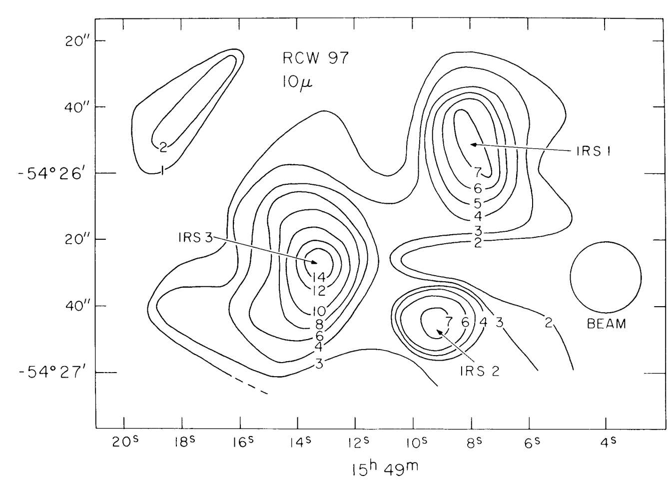

FIG. 8.—A 10-μ map of RCW 97. The flux density contours are in units of 14 = 4.76 × 10^{-25} W m^{-2} Hz^{-1} as measured with a 23″ diameter aperture. The 5-GHz position agrees with that of IRS 3.

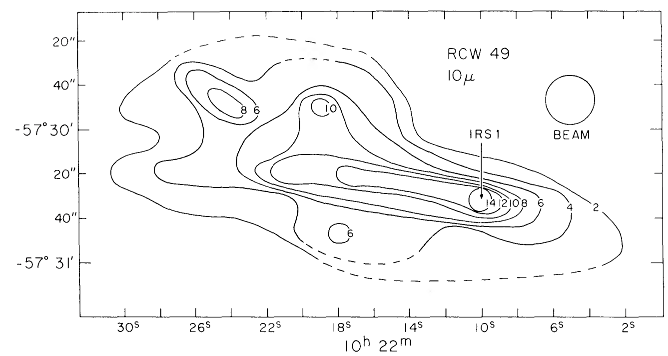

FIG. 9.—A 10-μ map of RCW 49. The flux density contours are in units of $14 = 4.94 \times 10^{-25}$ W m^{-2} Hz^{-1} as measured with a 23″ diameter aperture. The 5-GHz position is S and E of IRS 1.

0.1 f.u. could be determined with a 1′ diameter aperture. The available infrared data thus provide no information about the reddening. A nearby cluster of stars (just N of the infrared source) was studied by Westerlund (1960), who found it to suffer 6.5 mag of visual extinction and to lie at a distance of 6 kpc.

c) *W22* (*G353.2+0.9*)

The area mapped at 10 μ in figure 10 corresponds in position with the bright knot of nebulosity in the optical region NGC 6357. Both the optical and infrared sources are extended in the right ascension direction. The source G353.2+0.2, found by Emerson, Jennings, and Moorwood (1973), lies within 3′ of IRS 1.

The spectrum of W22/IRS 1 (fig. 1) is similar to that of RCW 49 and, in particular, has a relatively blue [10 μ] − [20 μ] color. Photometry at 10 and 20 μ of two points in W22 yielded the same color to within the errors. A 20-μ scan of a low signal-to-noise ratio through W22/IRS 1 is similar to the 10-μ scan, but size differences on the order of 30 percent cannot be ruled out.

d) *G285.3−0.0*

The 5-GHz radio continuum and 10-μ positions correspond with a knot of optical nebulosity in an outlying region of the η Carinae nebula (Shaver and Goss 1970). Scans at 10 and 20 μ have low signal-to-noise ratio, but together with multiaperture photometry at shorter wavelengths (fig. 11) indicate that the source consists of a relatively bright central component with extended wings. A scan at 2.2 μ with a 59″ aperture yields a size no greater than that at 10 μ.

e) *G298.2−0.3*

The kinematic distance of 12 kpc deduced for this source (Goss *et al.* 1972) places it among the most distant galactic sources known. A map of the intense 10-μ emission associated with G298.2−0.3 is presented in figure 12. Scans through the center at 10 and 20 μ (fig. 13) are nearly identical to one another. The multiaperture photometric data (fig. 11) show that the extent of the source at the shorter wavelengths is similar to that at the longer ones, although the fluxes measured at 1.65 and 2.2 μ with the two largest apertures are affected by the presence of two blue stars, which were found on 2.2-μ declination scans. These stars are probably not physically associated with the nebula, because their implied absolute visual magnitudes would then be brighter than −9. The nebular colors used in this paper were found with apertures small enough to exclude the two stars.

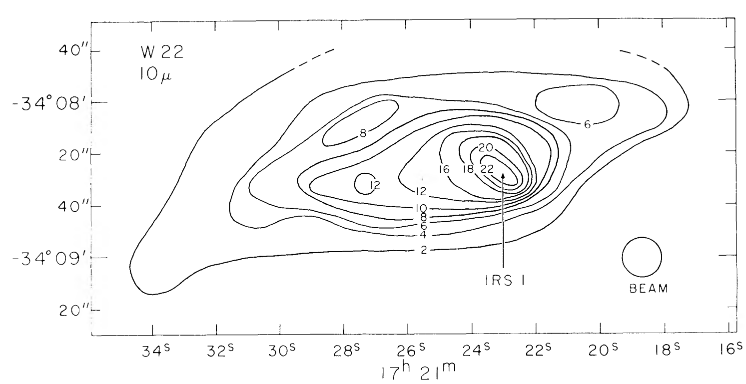

FIG. 10.—A 10-μ map of W22. The flux density contours are in units of $22 = 9.2 \times 10^{-25}$ W m^{-2} Hz^{-1} as measured with a 14″.5 diameter aperture. The 5-GHz position is 6^s E of IRS 1.

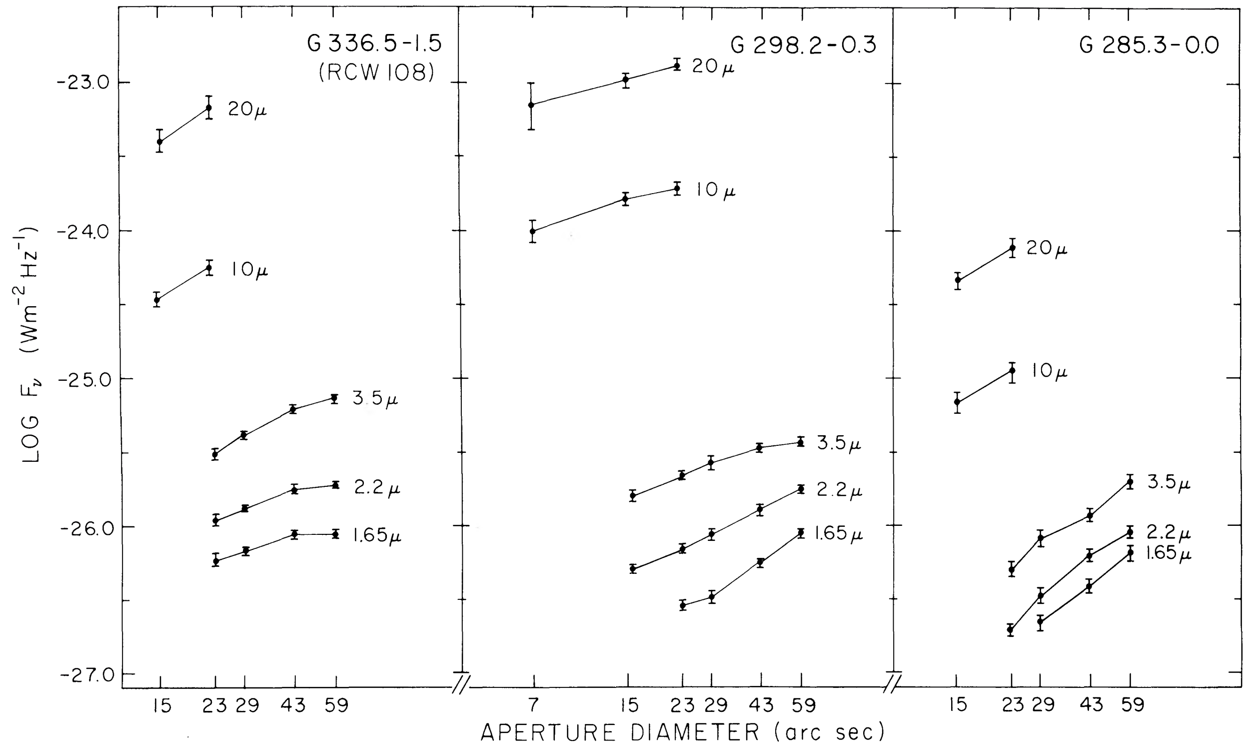

FIG. 11.—Relations between flux density and aperture diameter (plotted logarithmically) for three H II regions. The apparent bluing of the radiation from G298.2−0.3 at larger apertures is due to the presence of two blue stars found on 2.2-μ declination scans. The points for an object having constant surface brightness would lie on a 45° line in this plot.

The 1–25 μ luminosity of G298.2−0.3 is the highest measured for any galactic H II region. Its luminosity is nearly 3 times greater than that of G333.6−0.2 (Becklin *et al.* 1973*a*), a source which it closely resembles in spectral-energy distribution, apparent size, and surface brightness. Also, both H II regions consist of only one resolved infrared component, whereas other H II regions of comparable infrared luminosity, e.g., M17 (Kleinmann 1973), W3 (Wynn-Williams *et al.* 1972), and those discussed here, have complex structure. The apparent lack of structure may be due, in part, of course, to its distance.

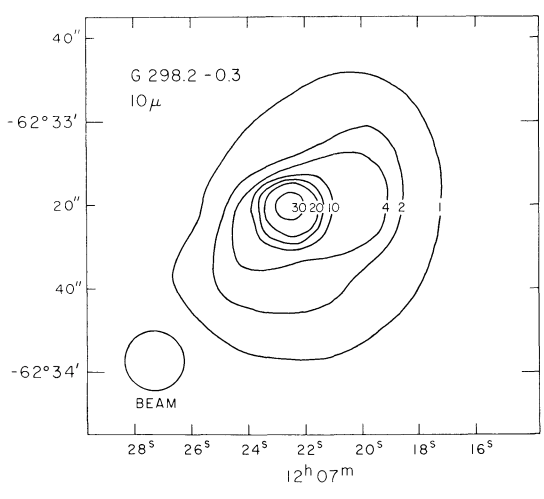

FIG. 12.—A 10-μ map of G298.2−0.3. The flux density contours are in units of 30 = 1.54 × 10^{-24} W m^{-2} Hz^{-1} as measured with a 14."5 diameter aperture. The 5-GHz position corresponds with the peak 10-μ position.

f) *G333.3−0.4*

Because of the low infrared surface brightness of this source away from the center, it was only possible to obtain scans through the position of peak 10-μ signal (fig. 14). Photometry with apertures of diameter 15″ and 22″ at 10 and 20 μ and 23″ and 59″ at 2.2 and 3.5 μ indicate the presence of an extended envelope of emission similar to that of G298.2−0.3. There is no significant dependence of color on aperture size.

g) *RCW 108* (*G336.5−1.5*)

The position of peak infrared emission corresponds with a bright knot of optical nebulosity, which in turn lies in the region of heavy obscuration that defines the western boundary of the optical nebula RCW 108 (NGC 6193). A map of the infrared source at 10 μ is shown in figure 15, and scans through the center at 10 and 20 μ are shown in figure 16. These data show that the infrared flux comes from a region not much larger than 1′, comparable with the radio size of 0.′7. This is one source for which the 20-μ size is significantly greater than the 10-μ size. Multiaperture photometric data for RCW 108 are presented in figure 11, which

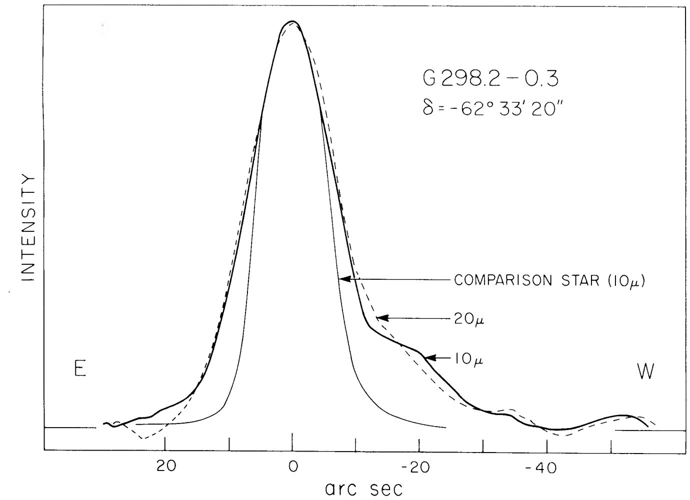

FIG. 13.—Deconvolved intensity scans of G298.2 − 0.3 at 10 and 20 μ. The 10-μ scan of a comparison star shown is similar to the corresponding scan at 20 μ.

shows that the [2.2 μ] − [3.5 μ] color is redder in the envelope than in the core, consistent with the trend of the 10- and 20-μ flux distribution. The multiaperture observations at 10 and 20 μ were not made with a sufficiently large range in aperture size to show the effect noted in figure 16.

RCW 108 is the only source for which the extrapolated radio flux is less than the 2.2-μ flux (fig. 1). This could be due to optical-depth effects at 5 GHz, an explanation that could also account for the positional disagreement noted in table 1.

h) *G351.6 − 1.3*

This source was studied at 5 GHz by Caswell (1972), who also found that the position of the OH emission (Robinson, Caswell, and Goss 1971) is within 0′.5 of the continuum position. The kinematic distance (table 1) is uncertain because of large peculiar velocities (Radhakrishnan *et al.* 1972). Brown and Broderick (1973) found that the source is smaller than 1′ at 85 GHz and measured a flux density of 5.8 f.u., one-fifth of that measured by Caswell (1972). They suggested that the radio source probably consists of several components. More recent interferometric measurements at 3.7 cm (Brown and Broderick 1974) show that G351.6 − 1.3 contains only one radio continuum component whose position and size (6″) agree with those of the infrared source. Emerson *et al.* (1973) measured the source in the region 40–350 μ and found a luminosity in this wavelength range of 19 × $10^5 L_\odot$ for a distance of 5 kpc. The present data consist of scans at 10 μ (see fig. 17) and a limited amount of multiaperture photometry. These data show that G351.6 − 1.3 is

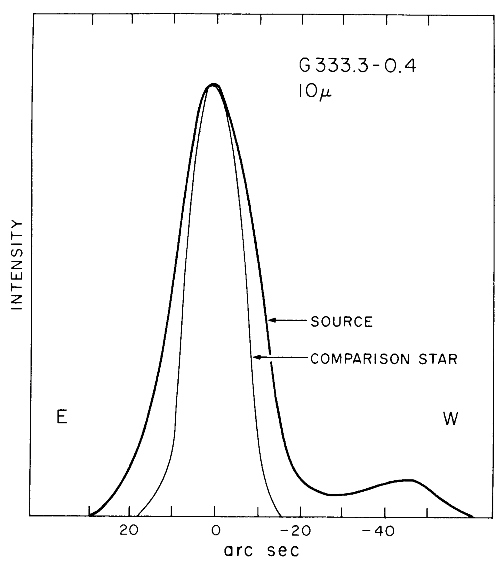

FIG. 14.—Deconvolved intensity scan of G333.3 − 0.4 at 10 μ. The source is seen to be considerably extended; there is also evidence for weak background emission to the west.

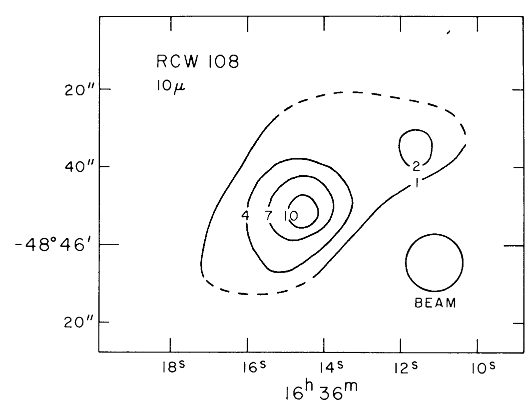

FIG. 15.—A 10-μ map of RCW 108. The peak lies on a small optical knot 3′ W of a bright ridge of optical emission that runs north-south. The flux density contours are in units of 10 = 4.2 × 10^{-25} W m^{-2} Hz^{-1} as measured with a 14″.5 diameter aperture. The 5-GHz position is S and E of the 10-μ position.

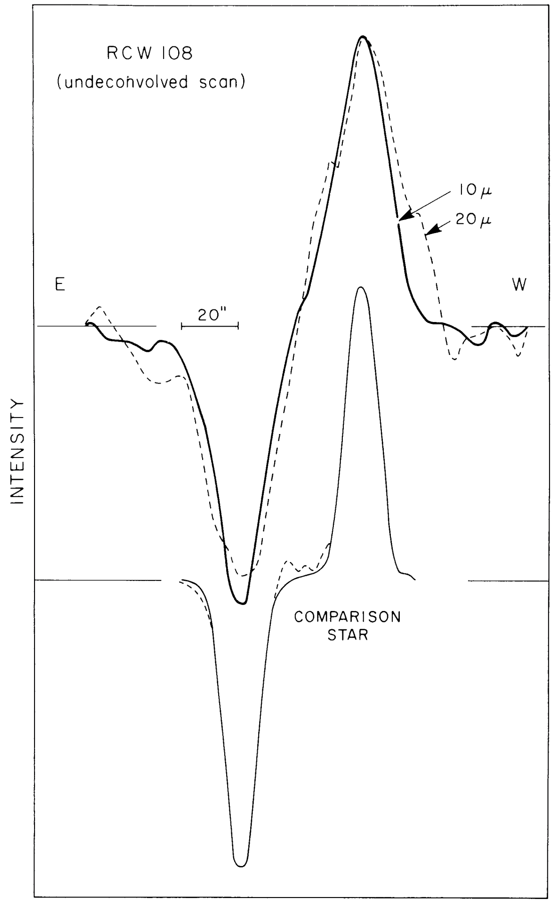

FIG. 16.—Undeconvolved intensity scans of RCW 108 at 10 and 20 μ. Scans of a star at these wavelengths are also shown, in order to emphasize the extended nature of RCW 108, and its size difference at 10 and 20 μ.

similar to G333.3 − 0.4 in structure, luminosity, and energy spectrum, but that the former is more centrally concentrated.

i) *W33* (*G12.8 − 0.2*)

A 10-μ scan through the infrared source associated with the radio continuum source (fig. 18) shows that most of the 10-μ flux comes from an unresolved object. Multiaperture photometry indicates the presence of only a very faint halo of emission. The weak 4.8-μ flux implies that W33 is quite unlike the other unresolved 10-μ source, RCW 57/IRS 1.

The radio data of Goss and Shaver (1970) and Schraml and Mezger (1969) indicate that W33 has a size of order 1′ and a flux density of between 25 and 30 f.u. at 5 GHz. Balick (1972) found only a small component (10″) at 8 GHz within W33, which emits 5 f.u. By comparison, the ratio of 2.2-μ flux as measured with apertures of diameter 59″ and 23″ is only 1.15, and is not likely to exceed 1.2 for a 10″ aperture. The lack of infrared emission outside the central unresolved source leads us to associate the infrared source with the compact radio source found by Balick (1972). The deficiency of 2.2-μ emission outside the center implies

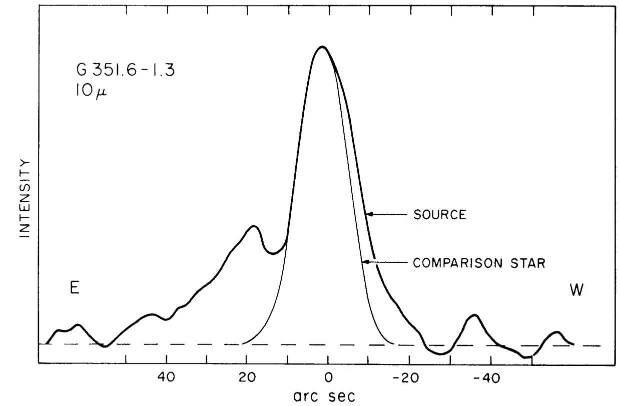

FIG. 17.—Deconvolved intensity scan of G351.6 − 1.3 at 10 μ. The similarity of the source and a star on the east side of the peak indicates that the source may consist of an unresolved source plus a moderately bright extended component.

that the outer regions suffer ⩾ 50 mag of visual extinction.

Figure 1 shows that the spectrum of W33 is similar to the spectra of the other infrared radio sources discussed in this Paper. However, with regard to both apparent brightness and intrinsic luminosity in the region 1.25–20 μ, W33 is the faintest of all the sources considered here and also has the lowest ratio of infrared to radio luminosity. This comparison is especially significant if we have in fact measured *all* of the infrared flux from the extended radio source. Thus, W33 is similar to DR 21, a source of high radio surface brightness and weak 10-μ emission (Wynn-Williams *et al.* 1974*a*).

j) *W31* (*G10.2 − 0.3*)

An area 6′ on a side around the continuum position given by Goss and Shaver (1970) was searched at 10 μ, but no emission to a level of 10 f.u. was found with an aperture 14″.5 in diameter. Since the continuum radio properties of W31 (high emission measure, small size,

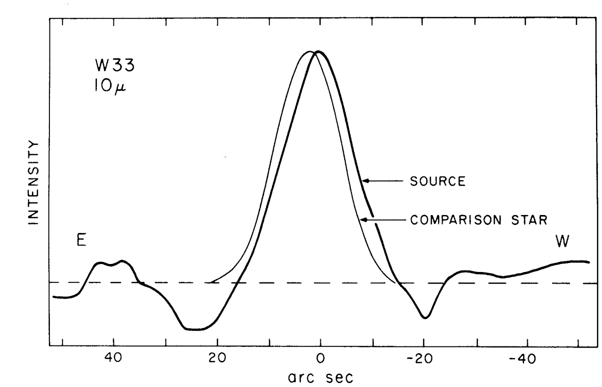

FIG. 18.—Deconvolved intensity scan of W33 at 10 μ. The scans of the source and that of a comparison star are indistinguishable and have been displaced horizontally for clarity. The noise level on this scan precludes a definitive statement about the background level.

TABLE 2

INFRARED COLORS OF RCW 38/IRS 2*

	[2.2 μ]	[1.25 μ] − [2.2 μ]	[1.65 μ] − [2.2 μ]	[2.2 μ] − [3.5 μ]
RCW 38/IRS 2 observed......	6.42	1.76	0.68	0.53
Early O star with $A_V = 12.8$	...	1.83	0.65	0.48

* Observations made with 16″ diameter aperture.

large flux density) are similar to those of W33, and both sources are bright at 100 μ (Hoffman, Frederick, and Emery 1971), we think that W31 is just a more extreme example of an infrared source with weak 1–25 μ emission.

IV. THE EXCITING STAR IN RCW 38

Table 2 gives the observed 2.2-μ mag and the colors of RCW 38/IRS 2. Also given are the predicted colors for an early O star having 12.8 mag of visual extinction. This value is consistent with the value of 10.7 mag derived from the nebular colors (table 1 and § VI). We have used the intrinsic colors given by Johnson (1966) and assumed a reddening law as given by van de Hulst's curve no. 15 (Johnson 1968). The good agreement between the observed and predicted colors leads us to conclude that RCW 38/IRS 2 is a highly reddened early type star or group of stars. For a distance of 1.5 kpc (Radhakrishnan *et al.* 1972), $M_V = -6.5$. If a smooth extrapolation of the 1.25, 1.65-, and 2.2-μ fluxes is made to an aperture of 10″ diameter, the colors, and hence the deduced extinction, do not change, but M_V becomes −6.1, corresponding to one O4 star (Conti 1973). The ionizing flux (Churchwell and Walmsley 1973) from such a star, or from a group of later spectral type O stars whose combined M_V is −6.1, is sufficient to account for the total 5-GHz radio flux. The characteristics of the star(s) are similar to those of the exciting star of H2-3 (Becklin *et al.* 1974).

V. RCW 57/IRS 1

The spectral energy distribution of the unresolved (<3″) source RCW 57/IRS 1 is shown in figure 7. The energy distribution is satisfactorily fitted by a 390° K blackbody suffering strong absorption at 10 μ. This spectrum is quite similar to those of W3/IRS 5 (Wynn-Williams *et al.* 1972) and the BN object in Orion (Becklin, Neugebauer, and Wynn-Williams 1973*b*), both of which have been proposed as candidates for protostars. Each of these objects has a very deep 10-μ absorption band which has been attributed to silicate particles (Gillett and Forrest 1973; Aitken and Jones 1973). The derived blackbody parameters for RCW 57/IRS 1 for $T = 390°$ K and a distance of 3.6 kpc are $4 \times 10^4 L_\odot$ and a radius of 200 a.u. These are similar to the values obtained for W3/IRS 5 and the BN object, and lead us to identify RCW 57/IRS 1 as a luminous protostar. Note that fitting a 390° K blackbody curve through the observed points makes no allowance for extinction at the shorter infrared wavelengths. The derived properties of RCW 57/IRS 1 are thus uncertain.

VI. REDDENING AND EXTINCTION

a) *Visual Extinction*

The extinction in front of an H II region can be estimated from the [1.65 μ] − [2.2 μ] color or from a comparison of the infrared fluxes with the extrapolated radio continuum if the radiation at 1.65 and 2.2 μ is primarily thermal emission from an ionized gas (Wynn-Williams *et al.* 1972; Willner, Becklin, and Visvanathan 1972). By using the spectral-energy distributions in figure 1 and the integrated 10-μ fluxes in table 1, and the association of average infrared colors with each source, we obtain integrated 2.2- and 1.65-μ fluxes. For those sources for which the radio size is larger than the infrared size, comparison of the infrared and radio fluxes gives an upper limit to the extinction. Thus, use of the [1.65 μ] − [2.2 μ] color is preferable.

The results of the two methods for calculating A_V are given in table 1. Van de Hulst's curve no. 15 (Johnson 1968), which is essentially the Whitford law, was used. *For those sources whose radio size is the same as the size of the region mapped in the infrared, the values of A_V derived by the two methods are in good agreement.* One exception is RCW 38, which has an extended background of moderately high radio surface brightness. Another is RCW 108, which we postulated to contain an optically thick radio component (§ III*g*). Note that a change in A_V of 5 mag corresponds to a change in the 2.2-μ flux or the 5-GHz flux of about 50 percent. This general agreement lends support to the assumptions used and indicates that no gross deviations from the Whitford law exist in the near-infrared.

The values of A_V found from the [1.65 μ] − [2.2 μ] color are usually larger than expected on the basis of 21-cm kinematic distances (table 1) and are considerably larger than values quoted by Georgelin and Georgelin (1970*a*, *b*), Georgelin, Georgelin, and Roux (1973), and Goss and Radhakrishnan (1969) for the optical components of some of the H II regions. As has been pointed out by others (cf. review by Wynn-Williams and Becklin 1974), much of this extinction probably arises in neutral clouds that surround the H II regions.

In the case of W22, the large visual absorption of 21 mag (table 1) is inconsistent with the presence of strong optical emission. Thus, either we are underestimating the 2.2-μ flux by a factor of 4 (which would reduce A_V to 4 mag), or most of the radio and infrared emission is coming from a region behind the optical nebulosity. Most of the obscuring matter would then necessarily lie between the radio source and the optical nebula. A similar model has recently been proposed for the Orion Nebula (Zuckerman 1973). The first alternative is reasonable since the infrared map covers an area smaller than the quoted radio size.

b) *Extinction at 10 μ*

Narrow-band measurements at 8.7, 11.7, and 12.6 μ reveal the presence of an absorption feature in the spectra of several of the sources. This absorption feature has been found in other H II regions and has been identified as a characteristic of silicate particles (cf. Gillett and Forrest 1973). We define the strength of this feature by

$$\tau(11.7\ \mu) = 0.8 \ln\left[\frac{F_\nu(12.6\ \mu)}{F_\nu(8.7\ \mu)}\right] - \ln\left[\frac{F_\nu(11.7\ \mu)}{F_\nu(8.7\ \mu)}\right].$$

This quantity measures the amount by which the measured flux at 11.7 μ lies below a continuum defined by the 8.7- and 12.6-μ measurements. Note that there are several effects that make this only a relative estimate rather than a true measure of the optical depth at 11.7 μ. First, and most importantly, the extinction may be affecting not a power-law continuum, but rather, a (silicate) emission feature that arises from dust within the H II region. Second, the possible presence of the 12.8-μ line of [Ne II] will cause an overestimate of $\tau(11.7\ \mu)$. Third, the values of $\tau(11.7\ \mu)$ systematically underestimate the optical depth of the feature, because there is probably extinction at 8.7 μ (cf. Aitken and Jones 1973), and the 11.7-μ filter is not centered on the silicate band. Inasmuch as the regions can be compared with one another, and the effects noted above do not vitiate the computation, then $\tau(11.7\ \mu)$ can be viewed as a true relative measure of the absorption at 11.7 μ. In figure 19*a* we plot $\tau(11.7\ \mu)$ against $\tau(H_2CO)$ as measured by Whiteoak and Gardner (1970) and Wilson (1972), where $\tau(H_2CO)$ refers to the line with a velocity corresponding to that of the continuum source. We have taken an average value of $\tau(11.7\ \mu)$ for the sources which were measured at several positions. Figure 19*a* shows a correlation in the sense that deeper absorption at 11.7 μ is associated with larger H_2CO optical depths. Unfortunately the 11.7-μ feature was not measured in W33, the source that has the largest $\tau(H_2CO)$ of those discussed here. In figure 19*b* we show $\tau(11.7\ \mu)$ versus the visual extinctions A_V, as found from the [1.65 μ] − [2.2 μ] colors. No correlation is evident on this plot. We have also attempted to correlate τ(OH) with $\tau(11.7\ \mu)$, however the results are ambiguous since OH data exist for only about half of the sources in figure 19*a*.

These results should be regarded as preliminary. New observations of more sources and with higher spectral resolution are underway.

Recent calculations by Dalgarno, Oppenheimer and Black (1973) have shown that the density of H_2CO depends roughly on the third power of the density of H. This indicates that H_2CO will be strongly concentrated in dense clouds of neutral gas rather than in interstellar space. In particular, one would expect that most of the H_2CO absorption observed in the direction of a high-density H II region would occur in the massive neutral clouds that are often associated with these objects. Whiteoak and Gardner (1970) suggested that "the existence of large optical depths requires an association of the absorbing cloud with the ionized region." Figure 19 then shows that most of the 11.7-μ absorption can be attributed to these same clouds.

On the other hand, a significant but largely unknown part of the [1.65 μ] − [2.2 μ] color must arise from *interstellar* reddening. The lack of correlation between this color and the 11.7-μ absorption may be taken as weak evidence that the silicate particles absorbing at 11.7 μ are not the ones primarily responsible for absorption at shorter wavelengths. This agrees with the results of Field (1974), who combined optical extinction data and abundance considerations to show that the silicate grains in the ζ Oph cloud can contribute only about 10 percent of the visual extinction.

Particularly good evidence supporting the general ideas above is provided by the observations of G298.2−0.3 in which both $\tau(H_2CO)$ and $\tau(11.7\ \mu)$ are small, and, per unit distance, are the smallest for all sources. From table 1, note that the visual extinction is 14 mag, consistent with a distance of 12 kpc, and no circumnebular cloud.

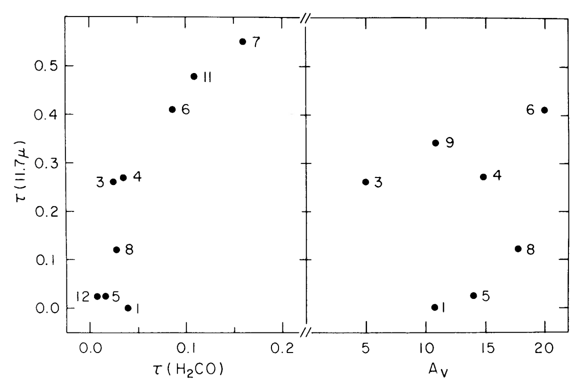

FIG. 19.—Comparison of the optical depth for extinction $\tau(11.7\ \mu)$ with (*a*) measured 6-cm formaldehyde optical depths and (*b*) values of A_V found from the [1.65 μ] − [2.2 μ] colors. The typical formal 1 σ_m uncertainty in $\tau(11.7\ \mu)$ is ± 0.06. No correlation of $\tau(11.7\ \mu)$ with interstellar extinction is evident. In this and the following plots, the numbers refer to the sources listed in table 1.

VII. DISCUSSION

a) *Source Structure*

At infrared wavelengths the H II regions we have observed consist of one or more compact components. Table 1 shows that generally the position of the strongest infrared component in each source corresponds with the radio position—discrepancies could be due to optical-depth effects at radio wavelengths. With the exceptions of RCW 38/IRS 2 and RCW 57/IRS 1 we assume that each of these infrared sources has an associated compact radio source. This has been shown explicitly for the core of G351.6−1.3, whose size and position have been measured at 85 GHz with a radio interferometer (Brown and Broderick 1974). Observationally, the similarity of the spatial distribution of flux at all wavelengths implies that the emitting dust (from 3 to 25 μ) and gas ($\leq 2.2\ \mu$) occupy the same volume. This has been shown explicitly for the regions discussed by Wynn-Williams *et al.* (1972, 1974*a*) for which aperture-synthesis radio observations are available.

As in the case for G333.6−0.2 and H2-3 (Becklin *et al.* 1973*a*, 1974), our observations indicate that

TABLE 3

DERIVED PARAMETERS OF H II REGIONS

No.	Source	θ (FWHP) (arc sec)	log [L(1–25 μ)/$L_\odot$] in FWHP	T_b(10 μ) (° K)	T_c(10–20 μ) (° K)	log τ_c	log (θD) (pc)	log ($M_{\rm H\,II}/M_\odot$)	log ($M_D/M_\odot$) + const
1A....	RCW 38/IRS 1	9	3.84	109	176	−2.20	−1.20	−0.77	−4.90
2A....	RCW 49/IRS 1	4	4.50	113	237	−2.89	−0.93	...	−5.06
3......	G285.3−0.0	18	3.83	84	182	−4.01	−0.36	+0.56	−5.03
4A....	RCW 57/IRS 2	22.5	4.61	94	165	−2.89	−0.41	+1.04	−4.00
4B....	RCW 57/IRS 3	19	4.40	97	166	−2.70	−0.47	+0.75	−3.94
5......	G298.2−0.3	9	5.69	110	180	−2.19	−0.28	+1.50	−3.06
6A....	RCW 97/IRS 1	21	3.81	86	182	−3.85	−0.46	+0.52	−5.07
6B....	RCW 97/IRS 3	13	3.83	92	188	−3.51	−0.68	+0.18	−5.17
7......	G333.3−0.4	16	4.22	91	168	−3.12	−0.53	+0.72	−4.47
8......	G333.6−0.2	9	5.47	126	195	−1.77	−0.71	+0.81	−3.48
9......	RCW 108	15	4.00	94	159	−2.74	−0.82	+0.45	−4.67
10......	H2-3	49	5.07	90	207	−3.89	+0.07	+1.93	−4.04
11......	G351.6−1.3	8.4	3.86	93	162	−2.89	−0.69	+0.13	−4.61
12......	W22/IRS 1	32	4.02	101	213	−3.26	−0.81	−0.27	−5.19
13......	W33	< 3	4.06	> 112	169	> −1.89	< −1.17	−0.40	−4.53

strong electron-density gradients exist in the gas and that, for each component, the dependence of N_e on physical radius r follows a $r^{-0.5}$ to r^{-1} law. Larson (1973) has shown that just after a star reaches the main sequence, the density of its dust and H II region follows a r^{-2} or $r^{-1.5}$ law. The observations are in the sense one would expect if density gradients get smoothed out as a young H II region expands.

Similar density gradients have been shown to exist in small northern H II regions (Frogel and Persson 1972; Persson and Frogel 1974*b*), several of which show a marked increase in the [2.2 μ] − [3.5 μ] color going from inside to outside. Such a dependence of color and radial distance is predicted for the later evolutionary stages of H II regions, and arises from a depletion of dust in the inner parts of the regions; cf. calculation by Davidson (1970).

b) *Temperatures and Optical Depths of the Emitting Dust*

As is usual for infrared emission from H II regions, the steep spectra cannot be fitted by a single temperature blackbody (e.g., Becklin *et al.* 1973*a*), and a range of grain temperatures is thus implied. The lack of significant spatial variations in the infrared colors for any given region means that grains radiating at different temperatures are not systematically segregated spatially and that there must exist a distribution of grain sizes.

Some of the derived properties of the sources and components of sources are listed in table 3. The FWHP sizes were in all cases determined from the scans made at 10 μ. The flux from within the FWHP size was determined from the contour maps, interpolation between multiaperture measurements, or, in a few cases, smooth extrapolation of the multiaperture measurements. The 10-μ brightness temperature T_b refers to this flux and the FWHP size. The 10/20 μ color temperatures T_c are calculated by assuming that the sources emit like gray bodies. A characteristic optical depth τ_c can be derived from $B_\nu(T_b) \equiv \tau_c B_\nu(T_c)$. This parameter does not represent a true optical depth, since it is expected that the radiating efficiency of the grains will be a strongly decreasing function of wavelength. This approach has the advantage, however, that within the assumption that all the sources are composed of similar particles, τ_c gives a *relative* measure of the grain optical depth in the 10- to 20-μ region, and does not involve detailed models for the emissivity or composition of the grains, neither of which is known to any degree of certainty. If the absorption efficiency $Q(a, \lambda)$ decreases toward longer wavelengths, as is the case for several hypothetical grain models, the grain optical depths are substantially increased. For example, if $Q(a, \lambda)$ varies as λ^{-1} rather than as λ^0, then the values of T_c (considered as a physical temperature) decrease, and every value of $\tau_c(10\ \mu)$ increases by a factor of 4. A λ^{-2} efficiency law produces another factor of 4 increase in $\tau_c(10\ \mu)$. These latter values of τ_c roughly obtain for silicate particles (considering only the 10- and 20-μ broad-band fluxes), since the absorption efficiency at 10 μ is about 4 times greater than that at 20 μ (Bromage, Nandy, and Khare 1973).

The physical parameters derived and conclusions drawn in this section do not differ from results for other H II regions; cf. Becklin *et al.* (1973*a*) and review by Wynn-Williams and Becklin (1974).

c) *Masses of Gas and Dust*

The mass of ionized hydrogen $M_{\text{H II}}$ in an H II region, of angular diameter θ (FWHP), and at a distance D can be obtained from a radio measurement at frequencies where the gas is optically thin, and is given by $M_{\text{H II}} \propto T_e^{0.75} S_\nu^{0.5} \nu^{0.05} D^{2.5} \theta^{1.5}$ (Schraml and Mezger 1969). Since the radio diameters are very crude, we have chosen to use infrared sizes and the 2.2-μ fluxes corrected for extinction via the [1.65 μ] − [2.2 μ] color rather than the radio data. In those cases where no 1.65-μ measurement was made, we have compared the 2.2-μ flux with the radio flux to estimate the extinction. The mass of dust M_D is given by $M_D \propto \tau_c(\theta D)^2$, where τ_c is the characteristic 10-μ optical depth discussed above. Then

$$M_D = \tfrac{1}{3}\pi \frac{a\rho_g}{Q(a, \lambda)} (\theta D)^2 \tau_c\,, \qquad (1)$$

where $Q(a, \lambda)$ is the absorption efficiency at wavelength λ, and ρ_g and a are the mass density and radius (assumed single valued) of a grain. The masses of ionized gas and emitting dust computed in this way are given in table 3 and compared in figure 20, where the constant has the value zero for $\rho_g = 1$ g cm^{-3}, $Q(a, \lambda) = 0.1$ and $a = 0.1\ \mu$.

The calculated masses of dust and gas are sensitive to the assumed distance, but the relative mass of gas

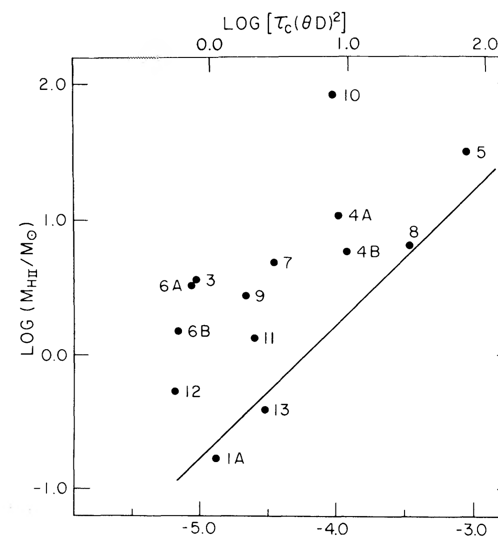

FIG. 20.—Comparison of the masses of ionized hydrogen with the masses of dust radiating in the 10- and 20-μ region. For $\tau_c(\theta D)^2$, θ is in arc sec and D in kpc. M_D has been calculated from equation (1); const = 0 for $a = 0.1\ \mu$, $\rho_g = 1$ g cm^{-3}, and $Q(a, \lambda) = 0.1$.

and dust $M_{\rm H\,II}/M_D$, which is proportional to $(S_\nu D/\theta)^{1/2}/\tau_c$, is not. The values of this ratio are more sensitive to uncertainties in the infrared parameter τ_c than to uncertainties in the size, distance, or flux. We note from figure 20 that there is a rough lower limit to the gas-to-dust ratio, independent of the absolute value of the mass of dust. This lower limit is represented by the straight line of slope unity. The values of $M_{\rm H\,II}/M_D$ in this graph thus obey the relationship

$$\frac{M_{\rm H\,II}}{M_D} \geq 1.7\,\frac{Q(a,\lambda)}{a\rho_g}\,, \tag{2}$$

if the gas and dust occupy the same volume, where ρ_g and a are in cgs units. This can be compared with the value of $\rho_{\rm H}/\rho_D$ (the space densities of gas and dust) derived optically (Aannestad and Purcell 1973);

$$\left(\frac{\rho_{\rm H}}{\rho_D}\right)_V \simeq 0.002\,\frac{Q_V}{a\rho_g}\,, \tag{3}$$

where Q_V is the *extinction* efficiency visually. For small ($0.05\,\mu$) silicate spheres, Bromage *et al.* (1973) give $Q(a, 10\,\mu) \simeq 0.15$, and $Q(a, 20\,\mu) \simeq 0.045$. Thus Q varies approximately as λ^{-2} for the 10- and 20-μ broad-band fluxes, and the values of τ_c and M_D increase by a factor of 16, as discussed previously. Then for $Q_V = 1$,

$$\frac{(\rho_{\rm H}/\rho_D)_{\rm IR}}{(\rho_{\rm H}/\rho_D)_V} \gtrsim 8\,\frac{(a\rho_g)_V}{(a\rho_g)_{\rm IR}}\,. \tag{4}$$

If the particles inside the H II region are similar to those in interstellar space, then this equation and figure 20 show that the dust may be depleted inside some of the H II regions relative to interstellar space. De Jong (1973) has shown that in order to have Lα heating dominate the direct stellar heating of the dust that is mixed in with the ionized gas (see below), such a depletion must occur. Models calculated by Wright (1973) also require a depletion of dust in the H II region. It is important to remember that this discussion concerns only the grains radiating at 10-20 μ, and does not apply to objects in which the far-infrared radiation originates within the ionized volume.

d) *Energetics*

The energetics of the sources are investigated by comparing the observed integrated flux from 1 to 25 μ with that available from Lα photons that are resonantly trapped within the ionized volume. This process has been most recently discussed by de Jong (1973) and Wright (1973). The observations imply that the emitting gas and dust occupy the same volume, as discussed in § VII*a* above. Thus, the distribution of N_e^2, which governs the emission at 2.2 μ (mostly free-free and in Lα, correlates with the 10-μ emission.

Resonance-line heating is the most efficient way to get energy, which derives ultimately from the central star, into the grains, since resonance photons cannot diffuse very far in physical space before they are absorbed by the dust. Fewer grains are then needed to radiate the available Lα energy, which is shared among all the grains in proportion to their absorption cross-sections at 1216 Å. The fact that some very hot particles are needed to provide the observed radiation at short wavelengths, around 3.5 μ, then results naturally as a consequence of sharing a fixed amount of energy among a small number of grains of various sizes.

The Lα luminosities of the sources (table 1) were found from the radio flux, the distance, and the formula of Rubin (1968), by using the approximation that, on the average, the number of Lα photons produced is two-thirds the number of primary ionizing photons absorbed within the H II region (Kaplan and Pikelner 1970). This approximation should be valid for the low ($\lesssim 10^4$) electron densities encountered in these nebulae.

The 1–25 μ luminosities listed in table 1 were computed from the spatially integrated 10-μ flux densities (also table 1) and the spectra (fig. 1) by assuming that F_ν varies as ν^{-n}, where n is determined from 10- and 20-μ flux densities. Since the values of n are large, the observed luminosity depends mainly on the flux at 20 μ, and only weakly on n. These luminosities are probably lower limits because very extended background emission of low surface brightness may be present. Purely statistical errors are $\sim$20 percent.

The integrated luminosities from 1 to 25 μ are compared with the Lα luminosities in figure 21. The plot shows that only in two cases (RCW 108 and W22) is the integrated infrared luminosity significantly greater than that available from Lα. This could be due to an underestimate of the Lα luminosity that would result if the sources were optically thick at 5 GHz. In all other cases, the luminosity in the Lα radiation field is comparable to the luminosity emitted from 1 to 25 μ, and supports the idea of Lα heating, at least for the sources discussed here.

The case of RCW 108 is interesting because the 20-μ size is larger than the 10-μ size and the 3.5-μ size is probably larger than the 2.2-μ size (figs. 11, 16). This

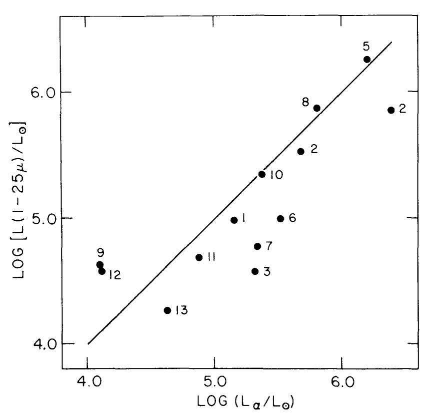

FIG. 21.—Comparison of integrated 1–25 μ luminosities with the luminosities available from Lα photons. The calculation of these quantities is described in the text. For sources numbered 2, 3, 7, and 11, we may be missing infrared flux from a background component. Correction for this effect will move the points closer to the straight line (equal luminosities). Sources 9 and 12 (RCW 108 and W22) are discussed further in the text.

is consistent with the idea that at least in this case a cloud of cool dust surrounds the ionized volume, and is heated by light from the exciting star(s) at $\lambda >$ 912 Å (cf. Wynn-Williams and Becklin 1974; Wright 1973). This then provides another possible explanation for the measurement (fig. 21) of more energy than is provided by Lα. These comments may also apply to other sources discussed by Wynn-Williams *et al.* (1974*a*), which are similar to RCW 108 in regard to the 2.2-μ/5-GHz flux density ratios, and/or whose sizes increase with increasing wavelength. It is interesting that the infrared sources in W22 and RCW 108 coincide with bright optical knots which probably have high emission measure.

In the two cases where we can isolate a star at wavelengths around $2\,\mu$, viz., H2-3 (Becklin *et al.* 1974) and RCW 38/IRS 2, the inferred stellar luminosity is consistent with that expected from a main sequence star whose ultraviolet output beyond the Lyman limit is not significantly different from that required to supply the observed radio flux. Therefore the dust cannot compete effectively with the gas for the primary ionizing photons. This provides further evidence that most of the heating within the H II region must be due to Lα. The bolometric luminosities of those sources discussed here that have been measured from 40 to 350 μ (Emerson *et al.* 1973) are consistent with the luminosities of the early-type star(s) required to give the observed radio fluxes. This has also been pointed out by Persson and Frogel (1974*a*) for K3-50 and by Johnson (1973) for other H II regions. This consistency provides additional evidence that, at least for these regions, the dust does not significantly affect the stellar ionizing flux contrary to the suggestion of Emerson *et al.* (1973). Rather, most of the far-infrared energy is derived from absorption of stellar photons with $\lambda > 912$ Å by dust that is just outside of the H II region (cf. Lemke and Low 1972; and Panagia 1973). This dust would be expected to exist in association with the massive H I complexes that usually surround H II regions and would be responsible for the large amounts of absorption observed shortward of 3.5 μ and in the 10-μ bandpass. Such a model has been discussed quantitatively by Wright (1973).

In contrast to the sources discussed in this paper, some of the sources discussed by Wynn-Williams *et al.* (1974*a*) may contain dust that competes with the gas for ionizing photons.

VI. SUMMARY AND CONCLUSIONS

We now summarize the infrared observations and conclusions based on them. The observations are generally in accord with what is known about other H II regions with associated infrared sources, as summarized by Wynn-Williams and Becklin (1974).

1. All of the H II regions have one or more compact infrared sources embedded in an extended region of lower surface brightness. Bright optical nebulosity corresponds in position with a few of the infrared/radio sources (e.g., W22).
2. On the average, the infrared colors are not functions of position in any given source, although some (e.g., RCW 108) are more extended at the longer wavelengths. The constancy of color implies that the H II, which is responsible for the emission at $\lambda \leq 2.2\,\mu$, and the dust, which radiates from 3.5 to 20 μ are well mixed.
3. Points 1 and 2 together imply that the spatial distributions of ionized gas and emitting dust (from 3.5 to 20 μ) are characterized by steep density gradients.
4. The 10-μ brightness temperatures and 10–20 μ color temperatures range from 84° to 126° K and from 159° to 237° K, respectively. The implied optical depths range from 10^{-2} to 10^{-4} for a Q independent of λ, and 4 or 16 times higher than these values if Q is proportional to λ^{-1} or λ^{-2}, respectively.
5. For those sources that have been observed in the infrared over an area corresponding in size to the radio continuum size, there is good agreement between values for the extinction derived from the [1.65 μ] − [2.2 μ] color and from the ratio of the 2.2-μ flux to the radio flux; this justifies use of the Whitford law in this spectral region. In most cases the extinction is large and thus is associated with the object itself.
6. The optical depth of an absorption feature in the 10-μ band, presumably due to silicates, correlates directly with $\tau(H_2CO)$ but not with the visual extinction. This is interpreted to mean that the silicate absorption occurs selectively in the circumnebular region where the largest concentration of H_2CO molecules is expected.
7. For the dust and gas referred to in point 2, above, there is a lower limit to the ratio M(H II)/M(dust). Even this lower limit is probably indicative of a deficiency of dust relative to gas when compared with the interstellar value.
8. The 1–25 μ luminosities range from 2×10^4 to $2 \times 10^6\,L_\odot$. In most, and perhaps all, cases this energy can be adequately accounted for by the absorption and reemission of resonantly trapped Lα photons by the dust grains mixed in with the ionized gas.
9. In RCW 38 we have been able to find the exciting star (IRS 2). As is the case for several other infrared/radio sources in which the source of excitation has been found, there is no evidence that any of the dust significantly affects the number of stellar ionizing photons that are available to the gas.
10. One source, RCW 57/IRS 1, is similar to the BN object in Orion and to W3/IRS 5—both of which have been advanced as candidates for protostars.
11. W33 may belong to a group of very young objects which includes at least W31 and DR21, and in which only a small amount of dust has been heated enough to radiate in the 10–20 μ region—most of the radiation occurs in the 50–350 μ region.

We are very grateful to Dr. H. W. Babcock for guest observer privileges at Las Campanas over the past 2 years. The study reported here would have been impossible to carry out without this observing time. We thank Srs. A. Zúñiga and A. Guerra for assisting with the observations. Drs. E. Becklin and G. Neugebauer were kind enough to allow us to use their unpublished data on RCW 38, RCW 57, and RCW 97.

We appreciate the critical readings of this manuscript by, and discussions with Drs. E. Becklin, E. Chaisson, T. de Jong, G. Field, G. Neugebauer, G. Shields, and G. Wynn-Williams. We thank Mr. E. Wright for pointing out an error in an earlier version of the paper. Ms. B. Langer and Mr. E. Franck patiently prepared the drawings and photographic reproductions. We thank Dr. R. Brown of NRAO for communicating his data on G351.6−1.3 prior to publication.

REFERENCES

Aannestad, P. A., and Purcell, E. M. 1973, *Ann. Rev. Astr. and Ap.*, **11**, 309.
Aitken, D. K., and Jones, B. 1973, *Ap. J.*, **184**, 127.
Balick, B. 1972, *Ap. J.*, **176**, 353.
Becklin, E. E., Frogel, J. A., Kleinmann, D. E., Neugebauer, G., Persson, S. E., and Wynn-Williams, C. G. 1974, *Ap. J.*, **187**, 487.
Becklin, E. E., Frogel, J. A., Neugebauer, G., Persson, S. E., and Wynn-Williams, C. G. 1973*a*, *Ap. J.* (*Letters*), **182**, L125.
Becklin, E. E., Neugebauer, G., and Wynn-Williams, C. G. 1973*b*, *Ap. J.* (*Letters*), **182**, L7.
Bromage, G. E., Nandy, K., and Khare, B. N. 1973, *Ap. and Space Sci.*, **20**, 213.
Brown, R. L., and Broderick, J. J. 1973, *Ap. J.*, **181**, 125.
———. 1974, *Ap. J.*, to be published.
Caswell, J. L. 1972, *Australian J. Phys.*, **25**, 443.
Churchwell, E., and Walmsley, C. M. 1973, *Astr. and Ap.*, **23**, 117.
Conti, P. S. 1973, *Ap. J.*, **179**, 181.
Dalgarno, A., Oppenheimer, M., and Black, J. H. 1973, *Nature Phys. Sci.*, **245**, 100.
Davidson, K. 1970, *Ap. and Space Sci.*, **6**, 422.
de Jong, T. 1973, *Bull. AAS*, **5**, 449.
Emerson, J. P., Jennings, R. E., and Moorwood, A. F. M. 1973, *Ap. J.*, **184**, 401.
Field, G. B. 1974, *Ap. J.*, **187**, 453.
Frogel, J. A., and Persson, S. E. 1972, *Ap. J.*, **178**, 667.
———. 1973, *Bull. AAS*, **5**, 408.
Georgelin, Y. P., and Georgelin, Y. M. 1970*a*, *Astr. and Ap.*, **6**, 349.
———. 1970*b*, *ibid.*, **7**, 133.
Georgelin, Y. M., Georgelin, Y. P., and Roux, S. 1973, *Astr. and Ap.*, **25**, 337.
Gillett, F. C., and Forrest, W. J. 1973, *Ap. J.*, **179**, 483.
Goss, W. M., and Radhakrishnan, V. 1969, *Ap. Letters*, **4**, 199.
Goss, W. M., Radhakrishnan, V., Brooks, J. W., and Murray, J. D. 1972, *Ap. J. Suppl.*, **24**, 123.
Goss, W. M., and Shaver, P. A. 1970, *Australian J. Phys.*, *Ap. Suppl.*, No. 14, p. 1.
Hoffmann, W. F., Frederick, C. L., and Emery, R. J. 1971, *Ap. J.* (*Letters*), **170**, L89.
Johnson, H. L. 1966, *Ann. Rev. Astr. and Ap.*, **4**, 193.
———. 1968, in *Nebulae and Interstellar Matter*, ed. B. M. Middlehurst and L. H. Aller (Chicago: University of Chicago Press), p. 167.
Johnson, H. M. 1973, *Ap. J.*, **182**, 497.
Johnston, K. J., Robinson, B. J., Caswell, J. L., and Batchelor, R. A. 1972, *Ap. Letters*, **10**, 93.
Johnston, K. J., Sloanaker, R. M., and Bologna, J. M. 1973, *Ap. J.*, **182**, 67.
Kaplan, S. A., and Pikelner, S. B. 1970, *The Interstellar Medium* (Cambridge, Massachusetts: Harvard University Press).
Kleinmann, D. E. 1973, *Ap. Letters*, **13**, 49.
Larson, R. B. 1973, *Ann. Rev. Astr. and Ap.*, **11**, 219.
Lemke, D., and Low, F. J. 1972, *Ap. J.* (*Letters*), **177**, L53.
Manchester, R. N., Robinson, B. J., and Goss, W. M. 1970, *Australian J. Phys.*, **23**, 751.
Panagia, N. 1973, *A.J.*, **78**, 929.
Persson, S. E., and Frogel, J. A. 1973, *Bull. AAS*, **5**, 318.
———. 1974*a*, *Ap. J.*, **188**, 523.
———. 1974*b*, *Ap. J.*, to be published.
Radhakrishnan, V., Goss, W. M., Murray, J. D., and Brooks, J. W., 1972, *Ap. J. Suppl.*, **24**, 49.
Robinson, B. J., Caswell, J. L., and Goss, W. M. 1971, *Ap. Letters*, **9**, 5.
Robinson, B. J., Goss, W. M., and Manchester, R. N. 1970, *Australian J. Phys.*, **23**, 363.
Rodgers, A. W., Campbell, C. T., and Whiteoak, J. B. 1960, *M.N.R.A.S.*, **121**, 103.
Rubin, R. H. 1968, *Ap. J.*, **154**, 391.
Schraml, J., and Mezger, P. G. 1969, *Ap. J.*, **156**, 269.
Shaver, P. A., and Goss, W. M. 1970, *Australian J. Phys.*, *Ap. Suppl.*, No. 14, p. 133.
Westerlund, B. 1960, *Ark. f. Astr.*, **2**, 419.
Whiteoak, J. B., and Gardner, F. F. 1970, *Ap. Letters*, **5**, 5.
Willner, S. P., Becklin, E. E., and Visvanathan, N. 1972, *Ap. J.*, **175**, 699.
Wilson, T. L. 1972, *Astr. and Ap.*, **19**, 354.
Wilson, W. J., Schwartz, P. R., Neugebauer, G., Harvey, P. M., and Becklin, E. E. 1972, *Ap. J.*, **177**, 523.
Wright, E. L. 1973, *Ap. J.*, **185**, 569.
Wynn-Williams, C. G., and Becklin, E. E. 1974, *Pub. A.S.P.*, **86**, 5.
Wynn-Williams, C. G., Becklin, E. E., and Neugebauer, G. 1972, *M.N.R.A.S.*, **160**, 1.
———. 1974*a*, *Ap. J.*, **187**, 473.
Wynn-Williams, C. G., Werner, M. W., and Wilson, W. J. 1974*b*, *Ap. J.*, **187**, 41.
Zuckerman, B. 1973, *Ap. J.*, **183**, 863.

Note added in proof.—Recent observations of the silicate absorption feature using several new filters in the 10-μ region confirm the correlation between silicate and formaldehyde absorption toward the sources described in the paper. W33, which has $\tau(H_2CO) \simeq 0.6$, has very deep silicate extinction, as expected. High spatial resolution observations at radio and infrared wavelengths are required to understand the nature of the clouds responsible for these absorption features.

Several additional H II regions were mapped at 10 μ. Of particular interest is the region around the young cluster NGC 3603. The 10-μ emission correlates with the presence of Hα emission, which forms an arc around the cluster. The details of these results will be published later.

Jay A. Frogel and S. Eric Persson
Center for Astrophysics, Cambridge, Massachusetts 02138